Editors' Suggestion | Featured in Physics

Microscale Hydrodynamic Cloaking and Shielding via Electro-Osmosis

Evgeniy Boyko,[1,4,‖] Vesna Bacheva,[1,2,‖] Michael Eigenbrod,[3,‖] Federico Paratore,[2,*] Amir D. Gat,[1,†] Steffen Hardt,[3,‡] and Moran Bercovici[1,§]

[1]*Faculty of Mechanical Engineering, Technion–Israel Institute of Technology, Haifa, 3200003 Israel*
[2]*IBM Research Europe, Säumerstrasse 4, 8803 Rüschlikon, Switzerland*
[3]*Department of Mechanical Engineering, Technische Universität Darmstadt, 64287 Darmstadt, Germany*
[4]*Department of Mechanical and Aerospace Engineering, Princeton University, Princeton, NJ 08544, USA*

(Received 1 December 2020; accepted 24 March 2021; published 6 May 2021)

We demonstrate theoretically and experimentally that injection of momentum in a region surrounding an object in microscale flow can yield both "cloaking" conditions, where the flow field outside the cloaking region is unaffected by the object, and "shielding" conditions, where the hydrodynamic forces on the object are eliminated. Using field-effect electro-osmosis as a mechanism for injection of momentum, we present a theoretical framework and analytical solutions for a range of geometrical shapes, validate these both numerically and experimentally, and demonstrate the ability to dynamically switch between the different states.

DOI: 10.1103/PhysRevLett.126.184502

Introduction.—Some 15 years ago, rapid progress was made in rendering objects invisible by cloaking them with metamaterials. After the development of a theoretical foundation for cloaking based on ray optics [1] and wave optics [2,3], experiments were reported that demonstrate invisibility cloaks in the microwave [4] and the infrared regime [5]. Effectively, these cloaks are shells composed of metamaterials with a tailor-made distribution of the effective dielectric permittivity and/or magnetic permeability, determined utilizing the invariance of Maxwell's equations under a transformation of the spatial coordinates [6]. Cloaking was also demonstrated by wrapping the object with a metasurface, a thin skin equipped with frequency selective patterns [7] or optical nanoantennas [8], replacing bulk metamaterials.

The concept of cloaking is not limited to optics and recently was extended to other scientific areas, including acoustic waves [9,10], conductive heat flux [11–14], stresses in an elastic medium [15–17], dc electric currents [18], and quantum mechanical matter waves [19]. Specifically, there are reports of hydrodynamic cloaks for both high and low Reynolds number flows. In terms of high Reynolds numbers, it was demonstrated how cloaking regions for waves propagating along liquid surfaces can be formed [20,21]. Of particular relevance to this work are hydrodynamic cloaks in the low Reynolds number regime. Urzhumov and Smith presented a theoretical concept for cloaking an object from three-dimensional unbounded fluid flow by embedding it in a medium with spatially varying porosity [22], and further extended their analysis to the case of a two-dimensional flow around a cylinder in a medium with mixed positive and negative permeabilities [23]. Park *et al.* [24] experimentally demonstrated a hydrodynamic metamaterial cloak inside a microchannel consisting of an arrangement of micropillars, showing a fivefold drag reduction on the object. More recently, there has been a growing interest in realizing metamaterial-less hydrodynamic cloaks through varying the channel depth around an obstacle [25] or locally introducing and withdrawing liquid [26].

Strictly speaking, in analogy to optics, "hydrodynamic cloaking" should refer to a state wherein the (flow) field external to some region around an object is unaffected by the presence of the object [see Fig. 1(b)]. However, several publications referred to the elimination of hydrodynamic forces on the object as cloaking [24]. To avoid such ambiguity, we here refer to the latter as "hydrodynamic shielding" [see Fig. 1(c)].

We here present a new theoretical approach and an experimental demonstration of hydrodynamic cloaking and shielding in a microfluidic chamber that does not rely on metamaterials. Instead, we take advantage of the fact that flow fields on small scales are completely governed by momentum sources at boundaries and can be linearly superposed. An effective way to create such momentum sources is electro-osmotic flow (EOF)—an electrokinetic phenomenon that generates flow due to the interaction of an applied electric field with native or induced net charge at liquid-solid interfaces [27]. Here, we focus on alternating-current field-effect electro-osmosis (ac FEEO) [28,29] as a mechanism for spatially inducing such charge, allowing spatial control of momentum injection around the object. We lay out a theoretical framework and closed-form analytical solutions allowing us to achieve both cloaking and shielding conditions for a range of geometrical shapes, and validate these both numerically and experimentally.

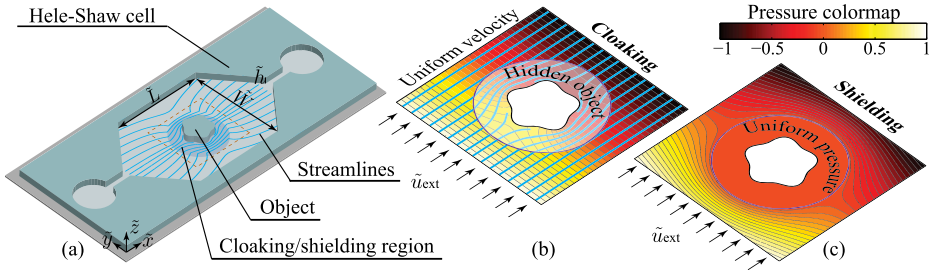

FIG. 1. Illustration of the concept of hydrodynamic cloaking and shielding and the configuration used for its modeling and experimental visualization. (a) The setup consists of a microfluidic chamber containing a pillarlike object with arbitrary cross-sectional geometry confined between two parallel plates. On the bottom plate, surrounding the object, is a gate electrode designed to cloak or shield the object. The chamber is filled with a liquid subjected to a pressure gradient resulting in a flow that in the native case curves around the object and exerts a force on it. By activating and controlling the EOF around the object, the velocity field and pressure distribution can be tuned either to cloak the object (b), such that the flow outside the electrode region remains uniform, or to shield the object (c) by creating a uniform pressure in its vicinity and eliminating the force on it.

The corresponding "cloaks" and "shields" presented here have simpler structures than their metamaterial equivalents, can be activated or deactivated on demand, and allow real-time transformation from one state to the other.

Theoretical modeling.—Figure 1 presents a schematic of the configuration used for modeling and experiments as well a conceptual illustration of the resulting hydrodynamic cloaking and shielding states. The setup consists of a pillarlike object with arbitrary cross-sectional geometry confined between two parallel plates of length $\tilde{L}$ and width $\tilde{W}$ separated by a small gap $\tilde{h}$ ($\tilde{h} \ll \tilde{L}$, $\tilde{W}$), forming a Hele-Shaw chamber [Fig. 1(a)]. As shown in Fig. 2, the cross-sectional geometry of the object is defined by $\tilde{r}_{\mathrm{obj}}(\theta) = \tilde{r}_0(1 + \beta f(\theta))$, where $f(\theta)$ is an arbitrary dimensionless smooth function and β is a parameter representing the geometrical deviations from a perfectly cylindrical shape with radius $\tilde{r}_0$.

The chamber contains a liquid subjected to pressure-driven flow with a far-field mean velocity of $\tilde{u}_{\mathrm{ext}}$ along the $\tilde{x}$ axis. Around the object, the flow field $\tilde{\boldsymbol{u}}$ and the pressure distribution $\tilde{p}$ are distorted by the object, resulting in curved streamlines and a hydrodynamic force on the object. We consider a configuration in which the object is surrounded by a cloaking or shielding region, wherein the zeta potential $\tilde{\zeta}_0$ on the lower and upper plates can be modified relative to the rest of the chamber. This control region has an outer radius $\tilde{r}_{\mathrm{cl,\,sh}}(\theta) = \tilde{r}_a + \beta\tilde{r}_0 g(\theta)$, where $g(\theta)$ describes the shape deviations from a circle with a radius $\tilde{r}_a$, satisfying $\tilde{r}_a > \tilde{r}_0$. We assume that the object is dielectric and acquires the same zeta potential $\tilde{\zeta}_0$ as the control region surrounding it. Upon application of an electric field $\tilde{E}$ along the $\tilde{x}$ axis, a nonuniform electro-osmotic flow is established in addition to the baseline flow, thus modifying the pressure distribution [30,31]. By controlling the surface potential in the control region, the pressure distribution can be tuned to eliminate pressure gradients within the region, thus creating shielding conditions [Fig. 1(c)] or to hide the object in a cloaking region, such that the flow outside is unaltered by the presence of the object [Fig. 1(b)].

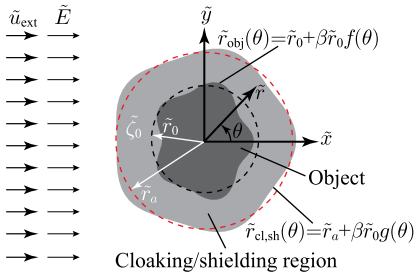

FIG. 2. Schematic illustration of the depth-averaged two-dimensional system used for theoretical modeling. $\tilde{r}_{\mathrm{obj}}(\theta)$ and $\tilde{r}_{\mathrm{cl,\,sh}}(\theta)$ represent the parametrization of the object shape and the cloaking and shielding region in which $f(\theta)$ and $g(\theta)$ describe the geometrical deviations from perfectly cylindrical and circular shapes, respectively.

Considering shallow geometries ($\tilde{h} \ll \tilde{r}_0 \ll \tilde{L}, \tilde{W}$), negligible fluidic inertia and assuming a thin electric double layer, the governing equations for the depth-averaged velocity $\langle \tilde{\boldsymbol{u}}_{\parallel} \rangle$, the pressure $\tilde{p}$, and the electrostatic potential $\tilde{\varphi}$ are (see Supplemental Material [32])

$$\langle \tilde{\boldsymbol{u}}_{\parallel} \rangle = -\frac{\tilde{h}^2}{12\tilde{\mu}} \tilde{\nabla}_{\parallel} \tilde{p} + \tilde{\boldsymbol{u}}_{\mathrm{slip}}, \tag{1}$$

$$\tilde{\nabla}_{\parallel}^2 \tilde{p} = \frac{12\tilde{\varepsilon}}{\tilde{h}^2} \tilde{\nabla}_{\parallel} \tilde{\varphi} \cdot \tilde{\nabla}_{\parallel} \langle \tilde{\zeta} \rangle, \tag{2}$$

and

$$\tilde{\nabla}_{\parallel}^2 \tilde{\varphi} = 0, \tag{3}$$

where $\tilde{\nabla}_{\parallel}$ and $\tilde{\nabla}_{\parallel}^2$ are the two-dimensional gradient and Laplacian in the $\tilde{x}$-$\tilde{y}$ plane and $\tilde{\boldsymbol{u}}_{\mathrm{slip}}$ is the depth-averaged Helmholtz-Smoluchowski slip velocity [27],

$$\tilde{\boldsymbol{u}}_{\mathrm{slip}} = \frac{\tilde{\varepsilon}\langle\tilde{\zeta}\rangle}{\tilde{\mu}}\tilde{\nabla}_{\parallel}\tilde{\varphi} \quad \text{for } \tilde{r}_{\mathrm{obj}} \le \tilde{r} < \tilde{r}_{\mathrm{cl,sh}}. \tag{4}$$

Here, $\tilde{\mu}$ is the fluid viscosity, $\tilde{\varepsilon}$ is the fluid permittivity, $\langle\tilde{\zeta}\rangle$ is the mean value of the zeta potential on the lower and upper plates, and $\tilde{\varphi}$ is the electrostatic potential related to the electric field $\tilde{\boldsymbol{E}}_{\parallel}$ through $\tilde{\boldsymbol{E}}_{\parallel} = -\tilde{\nabla}_{\parallel}\tilde{\varphi}$. We assume $\langle\tilde{\zeta}\rangle = \tilde{\zeta}_0$ within the cloaking and shielding region, and zero elsewhere.

To determine the conditions for cloaking and shielding analytically, we express the boundaries of the object and of the cloaking and shielding region assuming small deviations from a circle, $|\beta| \ll 1$, and assume that $f(\theta)$ and $g(\theta)$ are periodic functions that can be expressed as Fourier series expansions,

$$f(\theta) = \sum_{n=0}^{\infty}[a_n\cos(n\theta) + b_n\sin(n\theta)],$$
$$g(\theta) = \sum_{n=0}^{\infty}[d_n\cos(n\theta) + h_n\sin(n\theta)]. \tag{5}$$

While the object shape $f(\theta)$ and coefficients a_n, b_n are predefined, the shape of the cloaking and shielding region, given by $g(\theta)$ and coefficients d_n, h_n, is *a priori* unknown and is determined as a part of the solution. The above Fourier series will converge for any function differentiable everywhere in the domain (see additional comments for discontinuous functions in the Supplemental Material [32]).

To obtain a solution of the governing equations (1)–(4), we employ the domain perturbation method with regard to the small geometric parameter β, up to first order. The leading-order solution of this expansion corresponds to the case of a cylindrical object surrounded by an annular cloaking and shielding region, while the first-order correction represents the effect of the noncircular shape of the object. We solve the problem assuming an unbounded domain, enabled by the fact that the boundaries of the chamber are located far from the cloaking and shielding region [32,42]. Solving the uncoupled Laplace equation (3), we derive the leading- and first-order solutions for the electrostatic potential. Using Eq. (4), $\tilde{\boldsymbol{u}}_{\mathrm{slip}}$ can be expressed in the form $\tilde{\boldsymbol{u}}_{\mathrm{slip}} = \tilde{u}_{\mathrm{EOF}}G(\tilde{r}/\tilde{r}_0, f(\theta), \beta)$, where $\tilde{u}_{\mathrm{EOF}} = -\tilde{\varepsilon}\langle\tilde{\zeta}\rangle\tilde{E}/\tilde{\mu}$ and G is a nondimensional function that spatially varies in the cloaking and shielding region and vanishes elsewhere. Combining this result with Eqs. (1) and (2), we obtain closed-form solutions for the pressure and flow field in the leading and first orders.

The leading-order pressure distribution is [32],

$$\tilde{p} = \begin{cases} \dfrac{6\tilde{\mu}}{\tilde{h}^2\tilde{r}_a^2}[(\tilde{r}_a^2 - \tilde{r}_0^2)\tilde{u}_{\mathrm{EOF}} - 2\tilde{r}_a^2\tilde{u}_{\mathrm{ext}}]\left(\tilde{r} + \dfrac{\tilde{r}_0^2}{\tilde{r}}\right)\cos\theta\,, & \tilde{r}_0 < \tilde{r} < \tilde{r}_a\,, \\ \left[\dfrac{6\tilde{\mu}}{\tilde{h}^2\tilde{r}_a^2}[(\tilde{r}_a^4 - \tilde{r}_0^4)\tilde{u}_{\mathrm{EOF}} - 2\tilde{r}_a^2\tilde{r}_0^2\tilde{u}_{\mathrm{ext}}]\dfrac{1}{\tilde{r}} - \dfrac{12\tilde{\mu}\tilde{u}_{\mathrm{ext}}\tilde{r}}{\tilde{h}^2}\right]\cos\theta\,, & \tilde{r} > \tilde{r}_a\,. \end{cases} \tag{6}$$

For hydrodynamic cloaking, the flow field outside the cloaking region should be uniform, $\langle\tilde{\boldsymbol{u}}_{\parallel}\rangle = \tilde{u}_{\mathrm{ext}}\hat{\boldsymbol{x}}$. Since in this region the pressure and velocity are related through $\langle\tilde{\boldsymbol{u}}_{\parallel}\rangle = -\tilde{h}^2\tilde{\nabla}_{\parallel}\tilde{p}/12\tilde{\mu}$, this condition results in the requirement $\tilde{p} = -12\tilde{\mu}\tilde{u}_{\mathrm{ext}}\tilde{r}\cos\theta/\tilde{h}^2$ outside the cloaking region, which is satisfied when

$$\tilde{u}_{\mathrm{EOF}} = \frac{2\tilde{r}_a^2\tilde{r}_0^2}{\tilde{r}_a^4 - \tilde{r}_0^4}\tilde{u}_{\mathrm{ext}}. \tag{7}$$

For hydrodynamic shielding, we first note that in Hele-Shaw configurations, $\tilde{h}/\tilde{r}_0 \ll 1$, a scaling analysis shows that the viscous stress contribution $\tilde{\boldsymbol{\tau}}$ to the hydrodynamic stress tensor $\tilde{\boldsymbol{\sigma}} = -\tilde{p}\boldsymbol{I} + \tilde{\boldsymbol{\tau}}$ is negligible compared to the pressure contribution. The latter is also confirmed by our three-dimensional finite-element simulations [32]. We therefore neglect the viscous stress contribution and express the hydrodynamic force acting on the object as $\tilde{\boldsymbol{F}} = -\tilde{h}\int_0^{2\pi}\tilde{p}|_{\tilde{r}=\tilde{r}_{\mathrm{obj}}}\hat{\boldsymbol{n}}_{\mathrm{obj}}\tilde{r}_{\mathrm{obj}}\,d\theta$, where $d\tilde{S} = \tilde{h}\tilde{r}_{\mathrm{obj}}d\theta + O(\beta^2)$ is the surface element of the object and $\hat{\boldsymbol{n}}_{\mathrm{obj}} = \hat{\boldsymbol{r}} - \beta f'(\theta)\hat{\boldsymbol{\theta}} + O(\beta^2)$ is the outward normal to $\tilde{S}$. Considering the leading order and using Eq. (6), we find that the hydrodynamic force is eliminated when

$$\tilde{u}_{\mathrm{EOF}} = \frac{2\tilde{r}_a^2}{\tilde{r}_a^2 - \tilde{r}_0^2}\tilde{u}_{\mathrm{ext}}, \tag{8}$$

which also corresponds to uniform pressure in the entire shielding region.

To determine the shape of the cloaking and shielding region we use the first-order solution (see [32] for the detailed derivation). In the case of cloaking, we require the flow field outside the cloaking region to be uniform, and the resulting coefficients d_n, h_n that define the shape $g(\theta)$ are found from the recursive equations

$$d_n = r_a^2\frac{1 + r_a^{2n}}{1 + r_a^{2(n+2)}}d_{n+2} - \frac{1}{r_a^{n-1}}(a_{n+2} - a_n),$$
$$h_n = r_a^2\frac{1 + r_a^{2n}}{1 + r_a^{2(n+2)}}h_{n+2} - \frac{1}{r_a^{n-1}}(b_{n+2} - b_n), \tag{9}$$

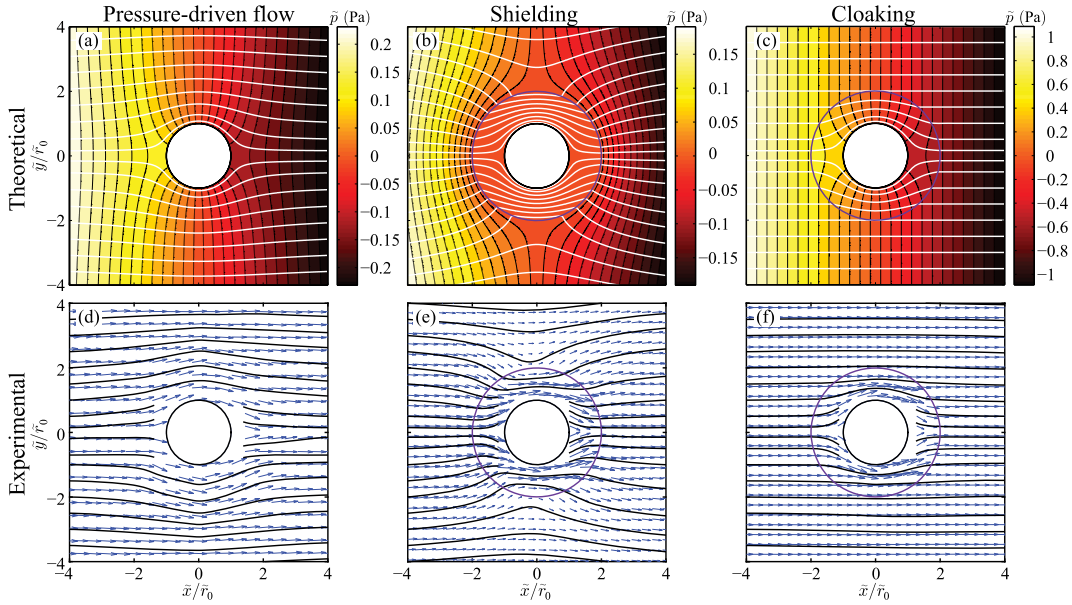

FIG. 3. Demonstration of hydrodynamic cloaking and shielding for the case of a cylindrical object. (a)–(c) Theoretical pressure distribution (color map) and streamlines (white lines) corresponding to (a) pressure-driven flow, (b) shielding with $\tilde{u}_{\mathrm{ext}} = 10.2\ \mu$m/s, and (c) cloaking with $\tilde{u}_{\mathrm{ext}} = 51.0\ \mu$m/s, satisfying Eqs. (8) and (7) when $\tilde{u}_{\mathrm{EOF}} = 27.2\ \mu$m/s. (d)–(f) Experimental flow fields (blue arrows) and resulting streamlines (black lines) corresponding to (d) pressure-driven flow with $\tilde{u}_{\mathrm{ext}} = 9.38\ \mu$m/s, (e) shielding with $\tilde{u}_{\mathrm{ext}} = 9.33\ \mu$m/s, and (f) cloaking with $\tilde{u}_{\mathrm{ext}} = 53.8\ \mu$m/s, for $\tilde{u}_{\mathrm{EOF}} = 27.2\ \mu$m/s. The cloaking and shielding region (purple line) is a circular annulus with $\tilde{r}_a = 2\tilde{r}_0$.

where $r_a = \tilde{r}_a/\tilde{r}_0$ and we choose the seed values for the coefficients d_{n+1}, d_{n+2}, h_{n+1}, h_{n+2} such that $d_{n_{\max}+1} = d_{n_{\max}+2} = h_{n_{\max}+1} = h_{n_{\max}+2} = 0$ and a_n, $b_n = 0\ \forall\ n > n_{\max}$, where $n = n_{\max}$ is the maximum summation index. Under this choice, there is a finite number of nonvanishing coefficients since Eq. (9) yields $d_n = h_n = 0$ for $n > n_{\max} + 2$. Together, Eqs. (7) and (9) define the shape and velocity magnitude of the hydrodynamic cloaking region.

In the case of shielding, to uniquely determine $g(\theta)$ we require the absence of a first-order force contribution and the fulfillment of the Helmholtz-Smoluchowski slip boundary condition at the object surface to obtain

$$d_n = \frac{a_n}{r_a^{n-1}}, \qquad h_n = \frac{b_n}{r_a^{n-1}}, \qquad n = 0, 1, 2, 3, \ldots. \tag{10}$$

Together, relations (8) and (10) define the shape and velocity magnitude of the hydrodynamic shielding region [46].

Figures 3(a)–3(c) present the theoretical pressure distribution (color map) and streamlines (white lines) for a cylindrical object subjected to pure pressure-driven flow, pressure-driven flow with shielding activated, and pressure-driven flow with cloaking activated. Under shielding conditions [Eq. (8)], the pressure inside the region surrounding the cylinder becomes uniform and the force on the object vanishes. Under cloaking conditions [Eq. (7)], the streamlines outside of the control region are straight, unmodified relative to the uniform far field, and undisturbed by the object. We validated the theoretical results based on a two-dimensional model by performing three-dimensional finite-element simulations, showing good agreement (see complete details in [32]). Using the numerical results, we calculate the hydrodynamic force on the cylindrical object, achieving a force reduction from 552 pN under pressure-driven flow to −50.4 pN under the shielding conditions. The negative value of the force indicates that the theory slightly overpredicts the magnitude of $\tilde{u}_{\mathrm{EOF}}$ required for perfect shielding. For the case of cloaking, the force decreases by approximately 28%, in good agreement with the theory that predicts a 25% reduction.

Experimental observations.—To experimentally demonstrate hydrodynamic cloaking and shielding, we used a 15 μm deep microfluidic chamber, connected to two reservoirs [Fig. 1(a)] and filled with an aqueous electrolyte 10) mM acetic acid, 1 mM NaOH). The object with a characteristic dimension of 100 μm is located at the center of the chamber and is surrounded at its base by a gate electrode covered with a dielectric and shaped as the desired cloaking and shielding region. We controlled the pressure-driven flow by imposing a pressure difference between the two reservoirs, and the EOF on top of the gate electrode by using ac FEEO [44,47]. In brief, the zeta potential on the gate electrode region is set by applying an ac potential difference between the gate electrode and the bulk liquid, in sync with a driving electric field along the chamber. The resulting time averaged EOF is zero outside the electrode region, whereas it can be dynamically

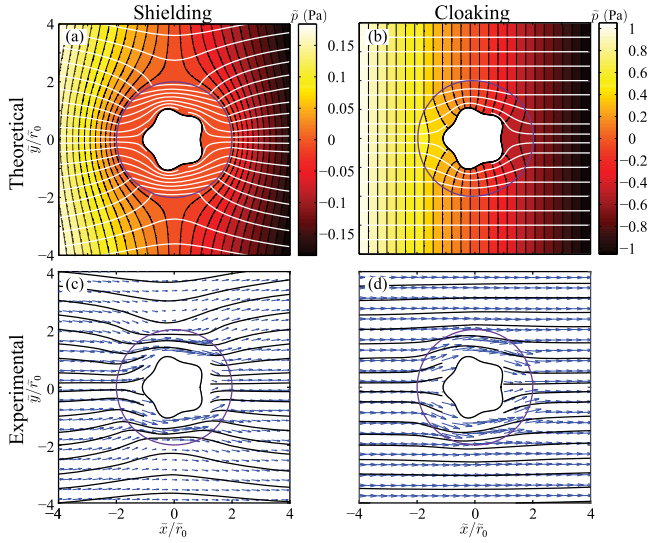

FIG. 4. Demonstration of hydrodynamic cloaking and shielding for the case of a flower-shaped object. (a),(b) Theoretical pressure distribution (color map) and streamlines (white lines) corresponding to (a) shielding with $\tilde{u}_{\mathrm{ext}} = 9.86\ \mu\mathrm{m/s}$, and (b) cloaking with $\tilde{u}_{\mathrm{ext}} = 49.3\ \mu\mathrm{m/s}$, satisfying Eqs. (8) and (7) when $\tilde{u}_{\mathrm{EOF}} = 26.3\ \mu\mathrm{m/s}$. (c),(d) Experimental flow field (blue arrows) and resulting streamlines (black lines) corresponding to (c) shielding with $\tilde{u}_{\mathrm{ext}} = 10.0\ \mu\mathrm{m/s}$, and (d) cloaking with $\tilde{u}_{\mathrm{ext}} = 48.1\ \mu\mathrm{m/s}$, for $\tilde{u}_{\mathrm{EOF}} = 26.3\ \mu\mathrm{m/s}$. The object (white region) is defined by $g(\theta) = -\cos(5\theta)$ and $\beta = 0.1$, and the cloaking and shielding region (purple line) is defined by Eqs. (9) and (10) with $\tilde{r}_a = 2\tilde{r}_0$.

controlled on top of the gate electrode by tuning the gate potential and the driving electric field.

We performed a series of experiments with different pressure-driven flow velocities at a fixed gate potential of 50 V and driving electric field of 200 V/cm, and visualized the flow field based on particle image velocimetry [45] using 1 μm fluorescent tracer particles. We measured the mean pressure-driven velocity $\tilde{u}_{\mathrm{ext}}$ by averaging velocity vectors far from the object where the flow is uniform and unaffected by the object. To obtain the value of $\tilde{u}_{\mathrm{EOF}}$ we recorded the flow field generated solely by the ac FEEO and fitted the resulting velocity map to a theoretically predicted flow field, yielding a value of $\tilde{u}_{\mathrm{EOF}} = 27.2\ \mu\mathrm{m/s}$ for the cylindrical object [32]. Using this value and Eqs. (7) and (8), we predict that the pressure-driven velocities satisfying the shielding and cloaking conditions are $\tilde{u}_{\mathrm{ext}} = 10.2\ \mu\mathrm{m/s}$ and $\tilde{u}_{\mathrm{ext}} = 51.0\ \mu\mathrm{m/s}$, respectively. To find the experimental value of $\tilde{u}_{\mathrm{ext}}$ required for cloaking and shielding, we tested different pressure-driven velocities $\tilde{u}_{\mathrm{ext}}$. We computed their deviation from the theoretical flow fields, and determined the $\tilde{u}_{\mathrm{ext}}$ value that yields the minimum deviation from the desired conditions. For shielding we obtained $\tilde{u}_{\mathrm{ext}} = 9.33\ \mu\mathrm{m/s}$ and for cloaking $\tilde{u}_{\mathrm{ext}} = 53.8\ \mu\mathrm{m/s}$, both in good agreement with the theoretical prediction. Figures 3(d)–3(f) present the experimentally observed flow fields (blue arrows) and resulting streamlines (black lines) for the native, shielded, and cloaked conditions. Movie 1 in Supplemental Material [32] demonstrates the ability to transition from cloaking to shielding conditions in real time by modifying the gate potential of the control region.

Cloaking and shielding of complex-shaped objects.—Applying our method to more complex shapes, we present in Fig. 4 hydrodynamic cloaking and shielding for the case of a flower-shaped object with $g(\theta) = -\cos(5\theta)$ and $\beta = 0.1$. Figures 4(a), 4(b) and Figs. 4(c), 4(d) present the theoretical and the experimental results, respectively, corresponding to shielding and cloaking conditions. Similarly to the case of a cylindrical object, the experimental values of $\tilde{u}_{\mathrm{ext}} = 10.0\ \mu\mathrm{m/s}$ for shielding and $\tilde{u}_{\mathrm{ext}} = 48.1\ \mu\mathrm{m/s}$ for cloaking, are in good agreement with the theoretical cloaking ($\tilde{u}_{\mathrm{ext}} = 49.3\ \mu\mathrm{m/s}$) and shielding ($\tilde{u}_{\mathrm{ext}} = 9.86\ \mu\mathrm{m/s}$) values. We further calculate the hydrodynamic forces on the object using the numerical simulations, finding that the force drops from 558 pN to −42.1 pN when the electro-osmotic shield is activated, demonstrating the applicability of our method to shield complex-shaped objects.

Conclusions and outlook.—We presented a new concept for the cloaking and shielding of objects in microscale flows, which uses injection of momentum via electro-osmosis, eliminating the dependence on complex metamaterial structures. We provided a complete theoretical framework that allows to compute the shielding or cloaking conditions for complex geometries, and validated it both numerically and experimentally. Furthermore, we showed the ability to turn the cloaking and shielding on and off on demand, as well as to transition from shielding to cloaking and vice versa in real time. Through its real-time adaptivity, this method introduces a new paradigm for hydrodynamic cloaking and shielding and goes beyond many existing cloaking concepts in other areas. A metamaterial can usually not be reconfigured, which means that the cloak cannot be adapted to changes in the incoming (electromagnetic, flow, temperature etc.) field. The characteristic timescale for flow modulations via the employed gate electrode is given by the momentum diffusion time $\tilde{h}^2/\tilde{\nu}$, where $\tilde{\nu}$ is the kinematic viscosity of the fluid. In our device, the momentum diffusion time is of the order of 10^{-4} s, allowing us to rapidly adapt to changes in the flow. To approach full adaptivity, it is conceivable to replace the existing gate electrode by an array of individually addressable electrodes that can be activated in a specific pattern corresponding to the instantaneous structure of the incoming flow.

The concepts of cloaking and shielding may also have very practical applications in the field of microfluidics. For example, shielding can be used as a type of hydrodynamic "tweezer," allowing us to either hold objects stationary in a flow, or control their in-plane motion. Controlling the force

distribution around an object may also prove interesting in inducing desired deformations on soft objects such as cells and small model organisms. This could be leveraged both as a diagnostics-sensing mechanism (e.g., the rigidity of cancer cells has been shown to significantly increase relative to healthy cells [48]) or as a mechanism for induction of mechanical stimulation.

M. B. thanks Professor Andrea Alu who saw our non-uniform electro-osmotic flow technology at a conference and was the first to insightfully suggest to explore its use as a cloaking mechanism. F. P. and V. B. acknowledge Dr. Govind V. Kaigala, Dr. Emmanuel Delamarche, and Dr. Heike Riel for their continuous support. This project has received funding from the European Research Council (ERC) under the European Union's Horizon 2020 Research and Innovation Programme, Grant Agreement No. 678734 (MetamorphChip). F. P. acknowledges the BRIDGE Proof-of-Concept program, Project No. 40B1-0 191549, funded by Innosuisse and the Swiss National Science Foundation. E. B. acknowledges the support of the Adams Fellowship Program of the Israel Academy of Sciences and Humanities, the Yad Hanadiv (Rothschild) Foundation, and the Zuckerman STEM Leadership Program.

*Corresponding authors.
federico.paratore@mat.ethz.ch
†Corresponding authors.
amirgat@technion.ac.il
‡Corresponding authors.
hardt@nmf.tu-darmstadt.de
§Corresponding authors.
mberco@technion.ac.il
‖These authors contributed equally to this work.

[1] U. Leonhardt, Optical conformal mapping, Science **312**, 1777 (2006).
[2] J. B. Pendry, D. Schurig, and D. R. Smith, Controlling electromagnetic fields, Science **312**, 1780 (2006).
[3] A. Alù and N. Engheta, Achieving transparency with plasmonic and metamaterial coatings, Phys. Rev. E **72**, 016623 (2005).
[4] D. Schurig, J. J. Mock, B. J. Justice, S. A. Cummer, J. B. Pendry, A. F. Starr, and D. R. Smith, Metamaterial electromagnetic cloak at microwave frequencies, Science **314**, 977 (2006).
[5] J. Valentine, J. Li, T. Zentgraf, G. Bartal, and X. Zhang, An optical cloak made of dielectrics, Nat. Mater. **8**, 568 (2009).
[6] H. Chen, C. T. Chan, and P. Sheng, Transformation optics and metamaterials, Nat. Mater. **9**, 387 (2010).
[7] A. Alù, Mantle cloak: Invisibility induced by a surface, Phys. Rev. B **80**, 245115 (2009).
[8] X. J. Ni, Z. J. Wong, M. Mrejen, Y. Wang, and X. Zhang, An ultrathin invisibility skin cloak for visible light, Science **349**, 1310 (2015).
[9] S. A. Cummer, B. I. Popa, D. Schurig, D. R. Smith, J. Pendry, M. Rahm, and A. Starr, Scattering Theory Derivation of a 3D Acoustic Cloaking Shell, Phys. Rev. Lett. **100**, 024301 (2008).
[10] S. Zhang, C. Xia, and N. Fang, Broadband Acoustic Cloak for Ultrasound Waves, Phys. Rev. Lett. **106**, 024301 (2011).
[11] C. Z. Fan, Y. Gao, and J. P. Huang, Shaped graded materials with an apparent negative thermal conductivity, Appl. Phys. Lett. **92**, 251907 (2008).
[12] T. Chen, C.-N. Weng, and J.-S. Chen, Cloak for curvilinearly anisotropic media in conduction, Appl. Phys. Lett. **93**, 114103 (2008).
[13] S. Narayana and Y. Sato, Heat Flux Manipulation with Engineered Thermal Materials, Phys. Rev. Lett. **108**, 214303 (2012).
[14] R. Schittny, M. Kadic, S. Guenneau, and M. Wegener, Experiments on Transformation Thermodynamics: Molding the Flow of Heat, Phys. Rev. Lett. **110**, 195901 (2013).
[15] M. Farhat, S. Guenneau, and S. Enoch, Ultrabroadband Elastic Cloaking in Thin Plates, Phys. Rev. Lett. **103**, 024301 (2009).
[16] N. Stenger, M. Wilhelm, and M. Wegener, Experiments on Elastic Cloaking in Thin Plates, Phys. Rev. Lett. **108**, 014301 (2012).
[17] T. Buckmann, M. Kadic, R. Schittny, and M. Wegener, Mechanical cloak design by direct lattice transformation, Proc. Natl. Acad. Sci. U.S.A. **112**, 4930 (2015).
[18] F. Yang, Z. L. Mei, T. Y. Jin, and T. J. Cui, dc Electric Invisibility Cloak, Phys. Rev. Lett. **109**, 053902 (2012).
[19] S. Zhang, D. A. Genov, C. Sun, and X. Zhang, Cloaking of Matter Waves, Phys. Rev. Lett. **100**, 123002 (2008).
[20] S. Zou, Y. Xu, R. Zatianina, C. Li, X. Liang, L. Zhu, Y. Zhang, G. Liu, Q. H. Liu, H. Chen, and Z. Wang, Broadband Waveguide Cloak for Water Waves, Phys. Rev. Lett. **123**, 074501 (2019).
[21] Z. Zhang, S. Liu, Z. Luan, Z. Wang, and G. He, Invisibility concentrator for water waves, Phys. Fluids **32**, 081701 (2020).
[22] Y. A. Urzhumov and D. R. Smith, Fluid Flow Control with Transformation Media, Phys. Rev. Lett. **107**, 074501 (2011).
[23] Y. A. Urzhumov and D. R. Smith, Flow stabilization with active hydrodynamic cloaks, Phys. Rev. E **86**, 056313 (2012).
[24] J. Park, J. R. Youn, and Y. S. Song, Hydrodynamic Metamaterial Cloak for Drag-Free Flow, Phys. Rev. Lett. **123**, 074502 (2019).
[25] F. Tay, Y. Zhang, H. Xu, H. Goh, Y. Luo, and B. Zhang, A metamaterial-free fluid-flow cloak, arXiv:1908.07169.
[26] O. Boyadjian, É. Boulais, and T. Gervais, Experiments on transformation microfluidics: Cloaking flow and transport without metamaterials, arXiv:2012.09931.
[27] R. J. Hunter, *Foundations of Colloid Science* (Oxford University Press, New York, 2001).
[28] R. B. M. Schasfoort, S. Schlautmann, J. Hendrikse, and A. van den Berg, Field-effect flow control for microfabricated fluidic networks, Science **286**, 942 (1999).
[29] S. Muthu, F. Svec, C. H. Mastrangelo, J. M. J. Frechet, and Y. B. Gianchandani, Enhanced electro-osmotic pumping with liquid bridge and field effect flow rectification, in *Proceedings of the 17th IEEE International Conference on Micro Electro Mechanical Systems.* Maastricht MEMS 2004 Technical

Digest (IEEE, New York, 2004), pp. 850–853, http://dx.doi.org/10.1109/MEMS.2004.1290720.
[30] E. Boyko, S. Rubin, A. D. Gat, and M. Bercovici, Flow patterning in Hele-Shaw configurations using non-uniform electro-osmotic slip, Phys. Fluids **27**, 102001 (2015).
[31] F. Paratore, E. Boyko, G. V. Kaigala, and M. Bercovici, Electroosmotic Flow Dipole: Experimental Observation and Flow Field Patterning, Phys. Rev. Lett. **122**, 224502 (2019).
[32] See Supplemental Material at http://link.aps.org/supplemental/10.1103/PhysRevLett.126.184502 for detailed theoretical derivations, experimental procedures and device geometry, details of the finite-element simulation, and supplemental figures and movies, which includes Refs. [33–45].
[33] J. Lyklema, *Fundamentals of Interface and Colloid Science, Volume II: Solid-Liquid Interfaces* (Academic Press, San Diego, CA, 1995).
[34] A. Ajdari, Electro-Osmosis on Inhomogeneously Charged Surfaces, Phys. Rev. Lett. **75**, 755 (1995).
[35] A. Ajdari, Generation of transverse fluid currents and forces by an electric field: Electro-osmosis on charge-modulated and undulated surfaces, Phys. Rev. E **53**, 4996 (1996).
[36] A. S. Khair and T. M. Squires, Surprising consequences of ion conservation in electro-osmosis over a surface charge discontinuity, J. Fluid Mech. **615**, 323 (2008).
[37] D. C. Prieve, J. L. Anderson, J. P. Ebel, and M. E. Lowell, Motion of a particle generated by chemical gradients. Part 2. Electrolytes, J. Fluid Mech. **148**, 247 (1984).
[38] A. S. Khair and T. M. Squires, Fundamental aspects of concentration polarization arising from nonuniform electrokinetic transport, Phys. Fluids **20**, 087102 (2008).
[39] L. G. Leal, *Advanced Transport Phenomena* (Cambridge University Press, Cambridge, England, 2007).
[40] H. Brenner, The Stokes resistance of a slightly deformed sphere, Chem. Eng. Sci. **19**, 519 (1964).
[41] J. Happel and H. Brenner, *Low Reynolds Number Hydrodynamics* (Springer Science & Business Media, New York, 1983).
[42] A. D. Gat, I. Frankel, and D. Weihs, A higher-order Hele-Shaw approximation with application to gas flows through shallow micro-channels, J. Fluid Mech. **638**, 141 (2009).
[43] H. Bruus, *Theoretical Microfluidics* (Oxford University Press Oxford, 2008).
[44] F. Paratore, V. Bacheva, G. V. Kaigala, and M. Bercovici, Dynamic microscale flow patterning using electrical modulation of zeta potential, Proc. Natl. Acad. Sci. U.S.A. **116**, 10258 (2019).
[45] W. Thielicke, PIVlab-particle image velocimetry (PIV) tool (https://www. mathworks. com/matlabcentral/fileexchange/27659-pivlab-particleimage-velocimetry-piv-tool), MATLAB Central File Exchange (retrieved April 24, 2019).
[46] An alternative and simplified derivation of the shielding condition for a weakly deformed cylinder can be found in M. Eigenbrod, The influence of boundary configurations on the dissipation and stability in fluids at low Reynolds numbers, Ph.D. thesis, Technische Universität Darmstadt, 2020, https://doi.org/10.26083/Tuprints-00017578.
[47] E. J. van der Wouden, D. C. Hermes, J. G. E. Gardeniers, and A. van den Berg, Directional flow induced by synchronized longitudinal and zeta-potential controlling ac-electrical fields, Lab Chip **6**, 1300 (2006).
[48] S. Suresh, Biomechanics and biophysics of cancer cells, Acta Biomater. **3**, 413 (2007).